Raman study of lysozyme amyloid fibrils suspended on super-hydrophobic surfaces by shear flow

proteins which escaped the cellular quality-control [12]. The presence of beta-sheet secondary structure can be confirmed by micro Raman spectroscopy, which is a non-destructive, label free technique especially suited for the localized biochemical analysis of biological samples. Appreciably, the results of Raman analysis can complement structural data obtained with other techniques such as NMR and x-ray spectroscopy, their most significant limitation being size (< 40 kDa) and the need for single crystals, respectively [13].

In Raman spectroscopy, the Amide I band position, largely shifting around 1650 cm^{-1}, is routinely used to detect beta-sheet composition of the proteins. The recent literature data agree in assigning beta-sheet secondary structure a Raman shift in the range 1665-1675 cm^{-1} [14, 15]. An upshift of the Amide I band is evidenced in the transition from functional protein to amyloid structure, where alpha-synuclein and insulin were considered [16, 17]. In 2007, a first report on functional amyloids derived from different types of silk fibers, highlighted the potential of polarized Raman spectroscopy, where beta-sheet secondary structure the Raman shift value in the range of 1666-1670 cm^{-1} [18]. They observed that the spectral width and the peak intensity ratio between the Amide I height of the polarized Amide I band collected in different scattering geometries to demonstrate that the main Raman tensor axis of the Amide I is highly oriented perpendicular to the fiber direction. A more recent polarized Raman spectroscopy study takes into consideration insulin amyloid fibers aligned on a planar substrate by the coffee ring stain effect [19, 20]. There, an increased intensity of the Raman peak centered at 1672-4 cm^{-1} emerges in the Raman spectrum when the fiber is aligned parallel to the laser polarization, an indication of the cross-beta structure of the fiber core.

Here we verify by micro Raman spectroscopy the beta-sheet composition of the hen egg white lysozyme (HEWL) after its conversion to amyloid fibrils. The samples were prepared suspended across the gaps between neighboring pillars, and thus in a substrate and debris free environment. In addition, and for each suspended singular fiber, we observe a clear dependence of the

68 intensity of the sheet secondary structure due to its orientation with respect to the
69 exciting laser polarization, with a three-fold counts increase when oriented parallel to the laser
70 polarization as compared to the perpendicular case. These results remark the ability of this technique to
71 align single molecules along one given direction. Fiber suspension by shear flow on super-hydrophobic
72 surfaces provides a fast and reproducible mean for the characterization of single molecules, purified form
73 the solution buffer and debris, which typically represent a serious problem in standard preparation for
74 laboratory analysis. The coupling of this preparation technique with Raman spectroscopy for the analysis
75 of the single suspended fiber is then a powerful combination for the study of any anisotropic fiber crystal,
76 where the structural characterization is not trivial by means of, e.g., x-ray crystallography or NMR.

77 ## Materials and Methods

78 ### 1. Super-hydrophobic surface fabrication

79 Super-hydrophobicity emerges as a result of the patterning and functionalization of the surface,
80 whose combination provides very high contact angle displayed by these substrates (>150 °). In this case,
81 the pattern is a sequence of concentric circular arrays of pillars with radial pitch of 18 µm, each of the
82 pillars having a diameter of 6 µm and height of 7 to 10 µm. To maintain a uniform surface coverage, the
83 number of pillars in each circular array was increased according to the recursive formula $N_i = N_{i-1} + 4$,
84 where N_i is the number of pillars of the ith circle. The patterning of the surface was obtained with a
85 combination of optical lithography and deep reactive ion etching (DRIE) technique. The original substrate
86 was a 4" standard Si <100> wafer. In the first step, the pillars pattern was defined by means of negative
87 optical lithography. The sample was then etched by means of DRIE (PlasmaLab System 100, Oxford
88 Instr.), with a final height of the pillars of about 10 µm. Finally, the functionalization of the surface with
89 hydrophobic material was achieved by the deposition of Perfluorodecyltrichlorosilane (FDTS) in a
90 Molecular Vapor Deposition System (MVD100E, Applied MST). FDTS in the presence of water reacts

with OH groups which are exposed at the surface of the oxidized Si, creating a monolayer of hydrophobic fluoro-carbon chain molecules bound to the sample surface. The functionalizing FDTS was dispensed together with water vapor in a vacuum pumped chamber of an MVD commercial system (MVD100E, Applied MST).

2. Lysozyme fibrils preparation

Lysozyme amyloid fibrils were produced starting from a solution of HEWL powder (Sigma) [10 mg/ml] in MilliQ water based on [21] $ F L G L I L F D W L R Q R I W K H V R O X W L R Q W R S+ q (v/v) of HCl [1N] in the solution. The mix was then immersed in a water bath at 60 °C for 120 h, until the formation of suitably long amyloid fibrils, as verified by AFM. No purification of the amyloid fibers was performed. The solution was then diluted ten times before depositing a 10 µl drop over the super-hydrophobic substrate with a hypodermic syringe microneedle. The drop was, thereafter, dried at room temperature and 50% humidity for 3 hours.

3. Sample characterization by AFM and SEM

The formation of amyloid fibrils at least 12 µm long (since this is the exact distance between the pillars edge in radial direction) was monitored by AFM. A 30 µl drop was withdrawn every 12 hours and spotted on a freshly cleaved mica sheet. It was let adsorb for 10 minutes and then rinsed thoroughly with MilliQ water. Finally it was N_2 dried and ready for measurement. JPK Nanowizard III mounted on inverted Olympus IX73 microscope was used for the measurement at relative humidity below 15%. XSC11 AFM probes (MikroMasch, Nanoworld AG) with nominal resonance frequency of about 150 kHz and nominal force constant of 7 N/m were run in tapping mode for the topography measurement.

After drop-casting the solution over the pillars top, we let it dry for 3 hours, then the deposition of the fibers was verified by a Quanta 200 FEG Scanning Electron Microscope (FEI) at 5 kV beam voltage and

64 pA current. Before imaging, the sample was sputter coated with 2 nm of Iridium, to avoid charging effects.

4. Raman spectroscopy of lysozyme amyloid fibrils

Laser micro-Raman spectroscopy was performed in confocal back scattering geometry by exciting the sample with 532 nm linearly polarized laser wavelength (Coherent Compass Sapphire Laser, 75 mW) at 4 mW power on a WiTec Raman spectrometer (Alpha300 RA) with Andor CCD detector (DU970N) cooled at -65 °C and a 100x objective (Zeiss, EC EPIPLAN NEOFLUAR, 0.9 NA). Measurements of the lysozyme powder dissolved in MilliQ water and lysozyme fibrils in acidic solution were performed after depositing the sample on a CaF_2 substrate to minimize signal background. The range of pillars height and spacing useful for effective deposition is chosen to be bigger than the focal length and lateral dimension of the focus of the objective. In this way the excitation volume is optimized to minimize the background from the silicon substrate. For the measurement of the fiber anisotropy, the sample was oriented at 0° (parallel) or 90° (perpendicular) with respect to the polarization of the excitation laser. Data analysis was carried out as follows: at least ten measurements per sample were acquired, baseline subtracted in the range 1100-1800 cm^{-1} (by grade 5 polynomial fitting) and averaged. Afterwards all the spectra were normalized to the Raman peak intensity at 1450 cm^{-1} to compare data. Amide I spectral region was fitted to a band described by a mixture of Lorentzian and Gaussian functions.

Results and Discussion

1. Amyloid fibers on SHS

Lysozyme amyloid fibrils suspended between pillars of a super-hydrophobic surface bear four major characteristics that make their study by Raman spectroscopy unique: they are made of single/few isolated

molecules, free from the presence of a substrate, clean and not contaminated by debris, and highly oriented along one given direction. This effect is obtained by the shear flow generated in the receding meniscus of the drop which contains the reaction solution (including fibrils, oligomers and native enzyme) and is evaporating over the micro-patterned SHS, and it was first demonstrated by De Angelis *et al.* [1]. In this work, cylindrical micro-pillars arranged in a circular pattern were used. Pillars inter-distance was 12 μm. The result of the dehydration process can be appreciated in Fig. 1: in Fig. 1a, four different drying areas emerge as a result of the evaporation of the drop maintained in quasi-spherical configuration by the SHS. The arrows indicate the drying direction, radial with respect to the center of the drop. Along the drying pattern, an area with salt residues is evident on the right bottom corner, preceding the area where the fibers are effectively extended hanging from the pillars edge (green line); this is then followed by a zone with a larger and amorphous residue on the pillars top (starting at the red line) followed by the edge of the collapsed drop (delimited by the blue line), where most of salt and fibers monomers, not long enough to extend across the pillars, are accumulated. This qualitative result partially supports the hypothesis that the SHS has a sieving effect on the drying solution. Fig. 1b-c are a sequence of zoom-in pictures better elucidating the formation of the fiber bundle hanging out from the top of a pillar in the part of Fig. 1a colored in green. The image of pillar top shows a darker area, where it is clearly visible the semicircular drying periphery of the solution bearing radial direction, indicated by the red arrows (Fig. 1b). A bundle of fibers is then formed, by coalescence of the fibers aided by the centripetal drying process (Fig. 1c). Following this organization process the fibers align over the interested area bridging consecutive pillars at a pillar-to-pillar distance of 12 μm. In the case shown in Fig. 2c, the generated fiber was quite thick, while in other cases thinner fibers were extended. For instance, in Fig. 2a, the fibers pinned at the edge of the pillar top have diameters of about 11 nm. This value includes the 2 nm of Iridium coating, such that the actual thickness is slightly reduced. The population distribution is then quite wide with fibers measuring also several tens of nanometers, mainly

depending on the distance from the center, such that a concentration effect is evident (the closer to the drop center, the more concentrated the solution, the thicker the fiber).

Amyloid fibrils can aggregate in different fashion to the limit, however, of the minimum size of the single amyloid fibril (called protofibril) at about 3 nm in diameter [22]. This effect of aggregation of multiple fibrils due to concentration can be better explained after considering the metrology of the single fibers as measured by the AFM. Fig. 2b is the AFM measurement topography performed at 120 h solution incubation time, after a drop of the mixture was spotted and dried over a freshly cleaved mica sheet: amyloid fibrils dimensions are 18 ± 3 nm of width, 3.4 ± 0.6 nm of height and a length of 19 ± 7 μm. The width originates actually from the profile measurement convolved with the tip shape, because it was not possible to deconvolve reasonably the signal. Thus, the measured height was taken into consideration. However it has to be pointed out that slight deformation of the fiber might depend on its adhesion to the mica surface, on the shrinking of the molecule due to dehydration and on the effect of the probe tip applying a force while performing the topography measurement. Moreover, the amyloid fibers have different shapes themselves, where the protofibril can organize into fibrils having from cylindrical to ribbon shape. Because the metrology of the amyloid fiber is beyond the scope of this work, we rely on the literature that reports an average radius of the amyloid protofibril, rather common among the different originating proteins, of about 3 nm, and we assume that the height of the fiber might be similar to this value. Given these premises, we can thus state that the height average measured by the AFM on the fibrils population is in agreement with the literature [23-25]. Amyloid fibers are composed of multiple protofilaments that are intertwined together into a twisted ultrastructure with regular periodicity. In these AFM measurements, two populations were found bearing each a twisting pitch of 76.5 ± 1.2 and 96.2 ± 1.7 nm. In conclusion, by comparing the AFM and the SEM measurement, we can argue that the thinnest fibers extended on the pillars top could likely be 2 to 4 protofibrils intertwined together, given the SEM diameter estimation.

2. Raman measurement of amyloid fibers on SHS

Lysozyme is an enzyme protein with antibacterial role and is commonly found in human secretions, macrophage and egg white. Due to its immunity importance and availability, lysozyme 3D structure and sequence have been among the first to be resolved. It has also been a model molecule in the early ages of Raman spectroscopy applied to biomedicine due to the presence of the main aminoacids in its sequence and of the S-S bond. Some major peaks characterize the laser Raman spectroscopy spectrum of a protein in the visible excitation range, related to specific aminoacids (e.g. Phenylanin ~1003 cm^{-1}; Tyrosine ~830, 850 cm^{-1}; Tryptophan ~763, 980, 1556 cm^{-1}), to specific covalent bonds (S-S ~510 cm^{-1}; C-H (def.) ~1450 cm^{-1} and C-N ~1130 cm^{-1}) and to secondary structure (Amide III ~1240 cm^{-1} and Amide I ~1650 cm^{-1}) [15]. Our interest particularly focuses on the secondary structure fingerprints, given that a globular protein, such as HEWL, will change its three dimensional structure by re-organizing the population distribution of its secondary structures in the conversion to amyloid protein. The Amide I band (Raman shift: 1620-1690 cm^{-1}), mainly due to the C=O stretching of the peptide carbonyl group, will be used in this work to describe the protein secondary structure in the visible excitation range. After the discovery that every protein can turn into amyloid fibril, lysozyme was readily used to study the onset of these pathological aggregates. The lysozyme powder is processed to obtain the amyloid fibrils, usually in denaturing conditions and high temperature. The result is the destabilization of the protein tertiary VWUXFWXUH LQWR DQ RSHQ JOREXODU IHDWXUH ZKLFK WKHQ U -strands, since this type of aggregation is energetically favored [26]. The structure of these assemblies has been somewhat controversial; however, a general pattern common too many proteins is nowadays accepted, where the FRUH RI WKH DP\ORLG ILEHU LV PDGH XS RI -sheets running perpendicular to the fiber and packed together by side-chains interactions [27] $VLGH IURP WKLV FRUH RWKHU VHFRQGDU\ VW -helices, random coils, loops, and other unordered structures are detected, depending on the sequence of the protein. Besides, proteins showing the tendency to form amyloid fibrils always possess a susceptible aminoacid

sequence which is prone to alteration [28, 29]. It has to be pointed out that different preparation conditions can give rise to amyloid polymorphs originating from the same protein, such that slight variability exists in the fibrils structure and related analysis outcomes. All of these characteristic secondary structures have been assigned specific Raman shifts in the Amide I band of the Raman spectrum. As a rule of thumb, the Amide I band will be mostly populated by the -sheet assigned peak, W K X V K D Y L Q J D F H [6, 7, 30]. In this work, by suspending bundles made of few fibrils between pillars, we expect a purified Raman signal unmistakably elucidating the secondary structure typical of the amyloid molecule.

In Fig. 3 the Raman spectra in the range 1500-1800 cm^{-1} of the lysozyme in MilliQ water (Lys-MQ), the lysozyme in the acidic solution after 120 h of incubation in hot bath (Lys-HCl) and the lysozyme fiber bridged across pillars (Fibril_Pill) are plotted. Focusing on the Amide I band in the range 1620-1690 cm^{-1}, an upshift of the Amide I peak is readily recognizable when moving from globular protein to amyloid fiber, where the peak apex moves from 1662 cm^{-1} to 1672 cm^{-1}. In particular, the curve Lys-MQ has a peak at 1662 cm^{-1}; the Lys-HCl has a peak centered at 1667 cm^{-1}; the Fibril_Pill bears a remarkably Q D U U R Z S H D N. This shift is already assigned in the literature to the transition from globular protein to amyloid fibril, where the peak at 1672 cm^{-1} P L J K W E H D V V L J Q H G W R W K H component of the Amide I region [17]. The measurement in which the laser polarization is parallel to the fiber is giving the better results in terms of the intensity R I W K H S H D N D V V R F L D W H G W R W fiber. Secondary structure, as compared to the spectrum obtained when the fiber is oriented perpendicularly to it: in fact, the peak intensity increases nearly three-folds (Fig. 4). This result V K R Z V W K D W D W -sheets are preferentially oriented perpendicular to the fiber axis, as previously demonstrated by Sereda *et al.* [19], in a polarized Raman study performed on insulin amyloid fibers aligned by the coffee ring stain effect. However in their work, there was a need for previous purification of the fibers and the analysis was not restricted to few molecules. Here we obtained the similar enhanced effect on the Raman spectrum, but

with the great advantage to provide with our method single bundles composed of few molecules that, while purified, are oriented according to the patterned surface. In fact, the drop-casted solution is populated by several species (globular enzymes, amyloid seeds, etc.), as it is shown in the AFM topography image in Fig. 2b. These species are largely removed from the extended fibers after the drop dries over the pillars, thanks to the sieving effect of the drying process on the SHS.

A deeper analysis of the results obtained from Raman spectroscopy on oriented fibers and electron microscopy characterization of these samples is beyond the scope of this publication and will be reported elsewhere in more detail.

Conclusions

In this work we have demonstrated a method to generate suspended amyloid fibrils highly oriented in a pre-defined direction by the use of a SHS. This method provides fibrils free of any contaminant and residual, decoupled from any supporting substrate, ready for further Raman or electron microscopy analysis. The sample is obtained by the shear flow generated at the rim of a drop, casted over a micro-patterned SHS. The receding meniscus combined with the shear flow and the pinning of the fibrils on pillars edge is responsible for the alignment and purification of the amyloid fibrils. In particular, we were able to suspend single/few amyloid fibrils of different diameters down to about 11 nm, as verified by the SEM imaging. The micro-Raman analysis of the sample, as expected, revealed a progressive upshift of the Amide I band main peak (from 1662 to 1667 to 1672 cm^{-1}) when the transition from pure-lysozyme to lysozyme-amyloid-fibrils solution (mix of fibers and oligomers) and to lysozyme amylo LG ILEULOV VXVSHQGHG RQ SLOODUV ZDV FRQVLGHUHG 7KL\ sheet secondary structure typical in amyloid fibrils. The distinctive anisotropic property of the amyloid fiber was also revealed with an enhanced Raman VLJQDO SHDN DW 1672 cm^{-1} after orienting the stretched fibrils parallel to the polarization of the incident laser. In conclusion, we would remark that this method

could be considered as well suited to characterize any type of anisotropic fiber crystals. We foresee the extension of the method for studying other protein molecules not only by Raman spectroscopy but also by transmission electron microscopies, both in diffraction and direct imaging configuration and x-ray crystallography. In fact, a single preparation technique, such as the dehydration on SHS device, provides a sample available for characterization under three complementary techniques, simplifying and reducing processing times. Future and alternative applications include, but are not limited to, the generation of patterned surfaces when bio-compatible material is desirable, thanks not only to the availability of the protein molecule (and eventual new synthesis of simpler sequences), but also to the possibility of chemical-biological modification of the starting material.

Acknowledgements

The authors acknowledge financial support from the KAUST start-up funding and from Italian Ministry of Health under the projects: Project no.: GR-2010-2320665 and Project no.: GR-2010-2311677.

References

[1] F. De Angelis, F. Gentile, F. Mecarini, G. Das, M. Moretti, P. Candeloro, M.L. Coluccio, G. Cojoc, A. Accardo, C. Liberale, R.P. Zaccaria, G. Perozziello, L. Tirinato, A. Toma, G. Cuda, R. Cingolani, E. Di Fabrizio, Breaking the diffusion limit with super-hydrophobic delivery of molecules to plasmonic nanofocusing SERS structures, Nat Photon 5(11) (2011) 682-687.

[2] F. Gentile, M. Moretti, T. Limongi, A. Falqui, G. Bertoni, A. Scarpellini, S. Santoriello, L. Maragliano, R. Proietti Zaccaria, E. di Fabrizio, Direct Imaging of DNA Fibers: The Visage of Double Helix, Nano letters 12(12) (2012) 6453-6458.

[3] F. Gentile, G. Das, M.L. Coluccio, F. Mecarini, A. Accardo, L. Tirinato, R. Tallerico, G. Cojoc, C. Liberale, P. Candeloro, P. Decuzzi, F. De Angelis, E. Di Fabrizio, Ultra low concentrated molecular

detection using super hydrophobic surface based biophotonic devices, Microelectron Eng 87(5–8) (2010) 798-801.

[4] F. Gentile, M.L. Coluccio, N. Coppedè, F. Mecarini, G. Das, C. Liberale, L. Tirinato, M. Leoncini, G. Perozziello, P. Candeloro, F. De Angelis, E. Di Fabrizio, Superhydrophobic Surfaces as Smart Platforms for the Analysis of Diluted Biological Solutions, ACS Applied Materials & Interfaces 4(6) (2012) 3213-3224.

[5] T. Limongi, F. Cesca, F. Gentile, R. Marotta, R. Ruffilli, A. Barberis, M. Dal Maschio, E.M. Petrini, S. Santoriello, F. Benfenati, E. Di Fabrizio, Nanostructured Superhydrophobic Substrates Trigger the Development of 3D Neuronal Networks, Small 9(3) (2013) 402-412.

[6] D. Bensimon, A.J. Simon, V. Croquette, A. Bensimon, Stretching DNA with a Receding Meniscus: Experiments and Models, Physical Review Letters 74(23) (1995) 4754-4757.

[7] M. Marini, A. Falqui, M. Moretti, T. Limongi, M. Allione, A. Genovese, S. Lopatin, L. Tirinato, G. Das, B. Torre, A. Giugni, F. Gentile, P. Candeloro, E. Di Fabrizio, The structure of DNA by direct imaging, Science Advances 1(7) (2015).

[8] M. Marini, G. Das, R. La Rocca, F. Gentile, T. Limongi, S. Santoriello, A. Scarpellini, E. Di Fabrizio, Raman spectroscopy for detection of stretched DNAs on superhydrophobic surfaces, Microelectron Eng 119 (2014) 151-154.

[9] M. Marini, T. Limongi, A. Falqui, A. Genovese, M. Allione, M. Moretti, S. Lopatin, L. Tirinato, G. Das, B. Torre, A. Giugni, F. Cesca, F. Benfenati, E. Di Fabrizio, Imaging and structural studies of DNA-protein complexes and membrane ion channels, Nanoscale (2017).

[10] M. Marini, M. Allione, B. Torre, M. Moretti, T. Limongi, L. Tirinato, A. Giugni, G. Das, E. di Fabrizio, Raman on suspended DNA: Novel super-hydrophobic approach for structural studies, Microelectron Eng 175 (2016) 38-42.

[11] F. Chiti, C.M. Dobson, Protein misfolding, functional amyloid, and human disease, Annu Rev Biochem 75 (2006) 333-66.

[12] C.M. Dobson, Protein folding and misfolding, Nature 426(6968) (2003) 884-90.

[13] M. Egli, Diffraction Techniques in Structural Biology: Overview for unit 7 “Biophysical Analysis of Nucleic Acids” in: Current Protocols in Nucleic Acid Chemistry, Current protocols in nucleic acid chemistry / edited by Serge L. Beaucage ... [et al.] CHAPTER 7 (2010) Unit-7.13.

[14] R. Tuma, Raman spectroscopy of proteins: from peptides to large assemblies, J Raman Spectrosc 36(4) (2005) 307-319.

[15] A. Rygula, K. Majzner, K.M. Marzec, A. Kaczor, M. Pilarczyk, M. Baranska, Raman spectroscopy of proteins: a review, J Raman Spectrosc 44(8) (2013) 1061-1076.

[16] K. Huang, N.C. Maiti, N.B. Phillips, P.R. Carey, M.A. Weiss, Structure-specific effects of protein topology on cross-beta assembly: studies of insulin fibrillation, Biochemistry 45(34) (2006) 10278-93.

[17] N.C. Maiti, M.M. Apetri, M.G. Zagorski, P.R. Carey, V.E. Anderson, Raman spectroscopic characterization of secondary structure in natively unfolded proteins: alpha-synuclein, Journal of the American Chemical Society 126(8) (2004) 2399-2408.

[18] T. Lefevre, M.E. Rousseau, M. Pezolet, Protein secondary structure and orientation in silk as revealed by Raman spectromicroscopy, Biophys J 92(8) (2007) 2885-95.

[19] V. Sereda, I.K. Lednev, Polarized Raman Spectroscopy of Aligned Insulin Fibrils, J Raman Spectrosc 45(8) (2014) 665-671.

[20] V. Sereda, M.R. Sawaya, I.K. Lednev, Structural Organization of Insulin Fibrils Based on Polarized Raman Spectroscopy: Evaluation of Existing Models, J Am Chem Soc 137(35) (2015) 11312-20.

[21] M.R.H. Krebs, D.K. Wilkins, E.W. Chung, M.C. Pitkeathly, A.K. Chamberlain, J. Zurdo, C.V. Robinson, C.M. Dobson, Formation and seeding of amyloid fibrils from wild-type hen lysozyme and a peptide fragment from the beta-domain, Journal of Molecular Biology 300(3) (2000) 541-549.

[22] L.C. Serpell, M. Sunde, M.D. Benson, G.A. Tennent, M.B. Pepys, P.E. Fraser, The protofilament substructure of amyloid fibrils, Journal of Molecular Biology 300(5) (2000) 1033-1039.

[23] J.L. Jiménez, E.J. Nettleton, M. Bouchard, C.V. Robinson, C.M. Dobson, H.R. Saibil, The protofilament structure of insulin amyloid fibrils, Proceedings of the National Academy of Sciences 99(14) (2002) 9196-9201.

[24] A.K. Chamberlain, C.E. MacPhee, J. Zurdo, L.A. Morozova-Roche, H.A.O. Hill, C.M. Dobson, J.J. Davis, Ultrastructural Organization of Amyloid Fibrils byAtomic Force Microscopy, Biophys J 79(6) (2000) 3282-3293.

[25] M. Moretti, C. Canale, M. Francardi, S. Dante, F. De Angelis, E. Di Fabrizio, AFM characterization of biomolecules in physiological environment by an advanced nanofabricated probe, Microsc Res Techniq 75(12) (2012) 1723-1731.

[26] D.R. Booth, M. Sunde, V. Bellotti, C.V. Robinson, W.L. Hutchinson, P.E. Fraser, P.N. Hawkins, C.M. Dobson, S.E. Radford, C.C. Blake, M.B. Pepys, Instability, unfolding and aggregation of human lysozyme variants underlying amyloid fibrillogenesis, Nature 385(6619) (1997) 787-93.

[27] T.R. Jahn, O.S. Makin, K.L. Morris, K.E. Marshall, P. Tian, P. Sikorski, L.C. Serpell, The common architecture of cross-beta amyloid, J Mol Biol 395(4) (2010) 717-27.

[28] A.P. Pawar, K.F. Dubay, J. Zurdo, F. Chiti, M. Vendruscolo, C.M. Dobson, Prediction of "aggregation-prone" and "aggregation-susceptible" regions in proteins associated with neurodegenerative diseases, J Mol Biol 350(2) (2005) 379-92.

[29] A. Lakshmanan, D.W. Cheong, A. Accardo, E. Di Fabrizio, C. Riekel, C.A.E. Hauser, Aliphatic peptides show similar self-assembly to amyloid core sequences, challenging the importance of aromatic interactions in amyloidosis, Proceedings of the National Academy of Sciences 110(2) (2013) 519-524.

[30] D. Kurouski, R.P. Van Duyne, I.K. Lednev, Exploring the structure and formation mechanism of amyloid fibrils by Raman spectroscopy: a review, The Analyst 140(15) (2015) 4967-80.

350 Figures and figure captions

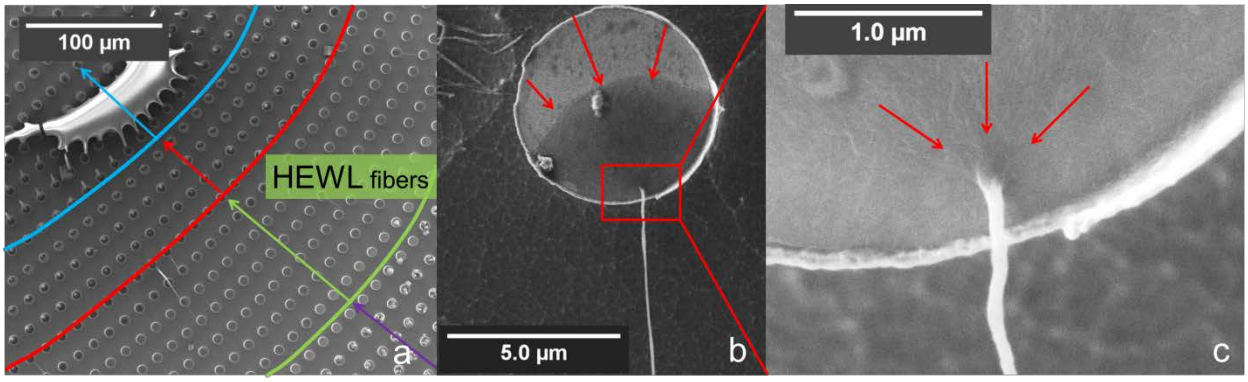

351

352 Fig. 1: SEM micrographs with cartoons elucidating the drying mechanism of the drop solution
353 spotted over the SHS. (a) A view over a large area which includes the side of the evaporated drop (top
354 left) and several drying areas evidenced by different marker colors. The green tag indicates the area were
355 the HEWL fibers are stretched over the pillars' top. The arrows indicate the drying direction; (b) a pillar
356 top with red arrows evidencing the drying shape and direction; (c) the area in the red square in (b) imaged
357 at higher magnification to show the coalescence of the fibers to one point (indicated by the red arrows)
358 where they are pinned out of the pillar top. The images were contrast and brightness corrected for better
359 visualization of the amyloid fibers.

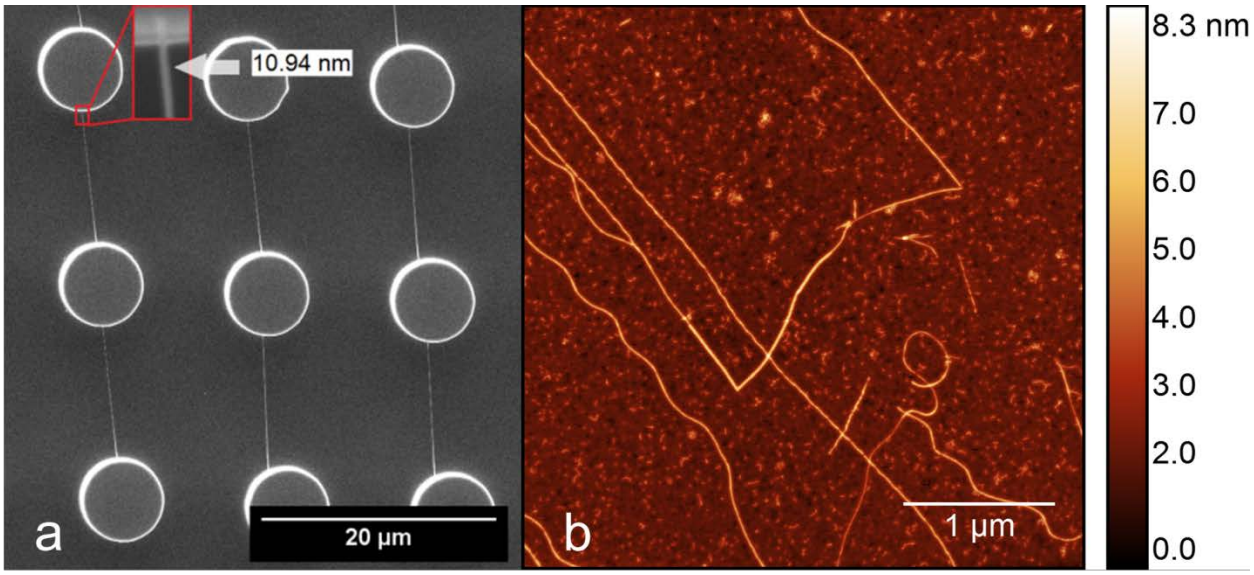

360

361 Fig. 2: (a) SEM micrograph of the suspended fibers over super-hydrophobic pillars. Minimum
362 diameter measured was about 11 nm (inset). (b) AFM topography of lysozyme amyloid fibrils deposited
363 on mica sheet after 120 hours of incubation. The height of the fibrils is about 3 nm.

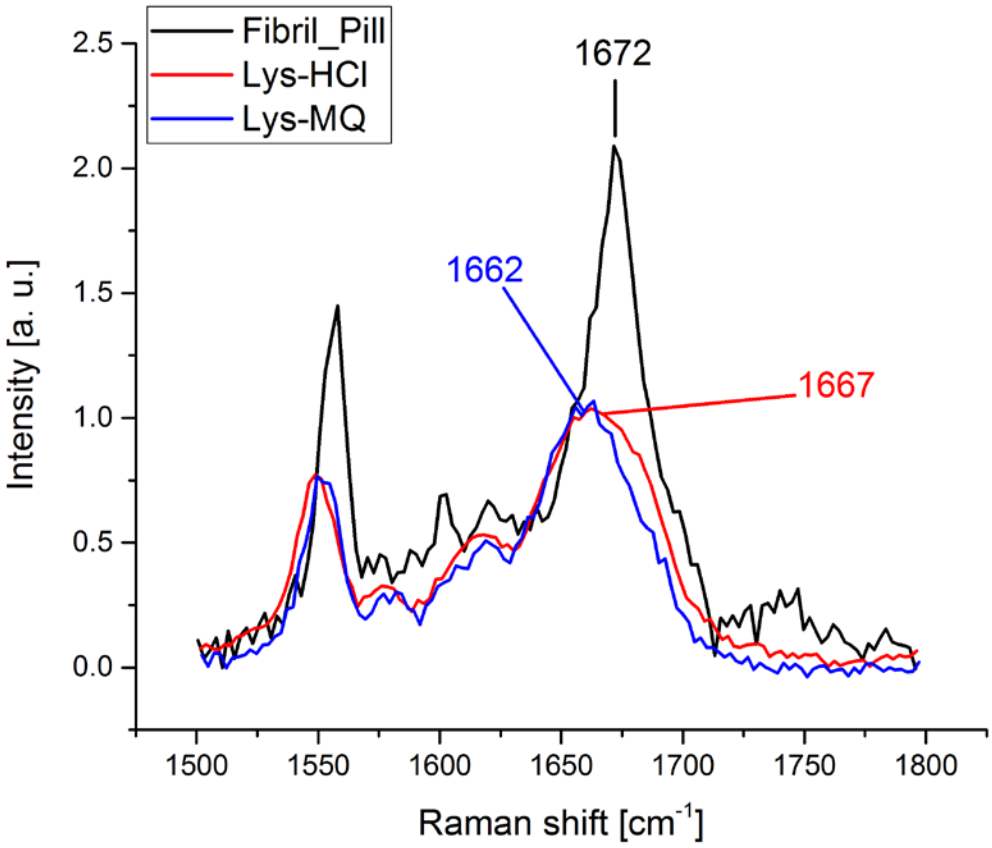

364

365 Fig. 3: Raman spectrum and peak assignment of the Amide I region for the HEWL in MilliQ water,

366 named Lys-MQ, in blue, HEWL in acidic solution, named Lys-HCl, in red and the HEWL fibers bridging

367 WKH SLOODUV WRS QDPHG)LEULOB3LOO LQ EOXH 7KH 5DPDQ VSHDN

368 assigned Raman peak was obtained by fitting Voigt function to a single peak in the Amide I band.

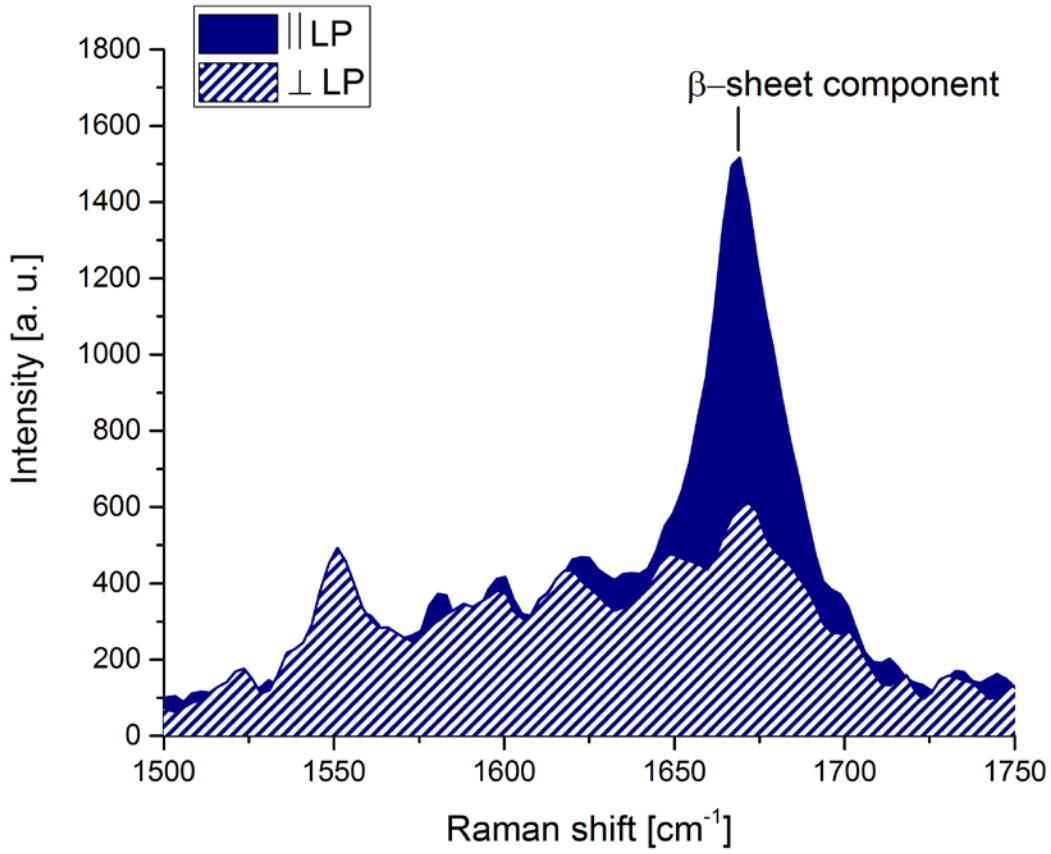

Fig. 4: Raman spectra of the amyloid fibers extended over the SHS with parallel (||LP, filled blue spectrum) and perpendicular (⊥LP, striped blue spectrum) orientation with respect to the exciting laser polarization (LP) in the region 1500 – 1800 cm^{-1}. The β-sheet component at 1672 cm^{-1} is remarkably enhanced in the case of the laser polarization parallel to the fiber direction.